applied sciences

MDPI

Article

Real-Time HIFU Treatment Monitoring Using Pulse Inversion Ultrasonic Imaging

Eui-Ji Shin [1], Byungwoo Kang [1] and Jin Ho Chang [1,2,*]

1 Department of Electronic Engineering, Sogang University, Seoul 04107, Korea; louishin@sogang.ac.kr (E.-J.S.); bill103@sogang.ac.kr (B.K.)
2 Department of Biomedical Engineering, Sogang University, Seoul 04107, Korea
* Correspondence: jhchang@sogang.ac.kr; Tel.: +82-2-705-4744

Received: 3 October 2018; Accepted: 8 November 2018; Published: 11 November 2018

check for updates

Abstract: Real-time monitoring of high-intensity focused ultrasound (HIFU) surgery is essential for safe and accurate treatment. However, ultrasound imaging is difficult to use for treatment monitoring during HIFU surgery because of the high intensity of the HIFU echoes that are received by an imaging transducer. Here, we propose a real-time HIFU treatment monitoring method based on pulse inversion of imaging ultrasound; an imaging transducer fires ultrasound twice in 0° and 180° phases for one scanline while HIFUs of the same phase are transmitted in synchronization with the ultrasound transmission for imaging. By doing so, HIFU interferences can be eliminated after subtracting the two sets of the signals received by the imaging transducer. This function was implemented in a commercial research ultrasound scanner, and its performance was evaluated using the excised bovine liver. The experimental results demonstrated that the proposed method allowed ultrasound images to clearly show the echogenicity change induced by HIFU in the excised bovine liver. Additionally, it was confirmed that the moving velocity of the organs in the abdomen due to respiration does not affect the performance of the proposed method. Based on the experimental results, we believe that the proposed method can be used for real-time HIFU surgery monitoring that is a pivotal function for maximized treatment efficacy.

Keywords: high-intensity focused ultrasound; HIFU surgery; HIFU treatment guidance; pulse inversion; ultrasound harmonics; HIFU interference cancellation; organ motion

1. Introduction

High-intensity focused ultrasound (HIFU) has attracted considerable attention as a non-invasive surgical tool; its applications range from cancer to brain disease treatment such as Alzheimer's disease [1,2] and cosmetic treatment such as skin tightening [3,4]. A pivotal element in HIFU surgery is an image guidance method for both pre-operative and intra-operative sessions. Magnetic resonance imaging (MRI) is typically used to identify a target lesion and determine a surgical plan pre-operatively. In an intra-operative session, either MRI or ultrasound is used for safe and accurate treatment guidance: estimation of temperature in treatment area [5,6], HIFU focus targeting [7,8] and motion tracking [9,10], each with their own advantages and disadvantages. Compared to MRI, ultrasound imaging is the preferred guidance method for HIFU focus targeting and motion tracking because these functions require real-time imaging capability. Additionally, this method has the ability to monitor lesion change in real time in response to HIFU [11].

Because HIFU is a high-intensity signal, its echoes received by an imaging transducer have an amplitude higher than imaging echoes. The HIFU echoes are called HIFU interference signals in this paper. For this reason, the structural information in ultrasound images is inevitably buried in HIFU interference signals. This is so because an ultrasound imaging transducer receives not only imaging signals but also HIFU interference signals although the operating frequency of the imaging transducer is different from that of the HIFU transducer. To fully realize the benefits mentioned above, it is necessary to remove HIFU interference from imaging signals, so that it is possible to acquire the ultrasound images of the treatment area during HIFU surgery. To eliminate the HIFU interference pattern in ultrasound images, various methods have been proposed: HIFU excitation synchronized with ultrasound imaging sequence [7,12], imaging signal acquisition during time periods for which HIFU is not delivered [13], coded excitation for imaging in conjunction with filtering [14,15]. However, each method has different optimal condition of HIFU pulse length (i.e., either short or long pulse length) to achieve their best performance.

Recently, we have proposed the HIFU interference cancellation method using pulse inversion, which does not have a constraint on HIFU pulse length theoretically [16,17]. Similar to the general pulse-inversion method used in ultrasound tissue harmonic imaging [18], two HIFU pulses with phase 0° and 180° are transmitted in the previously proposed method. Since two sets of echoes received by an ultrasound imaging transducer contain both HIFU interference and imaging signals for one image scanline, the fundamental and odd-harmonic components of HIFU interference can be eliminated after adding the two sets of echoes; only imaging signals remain after band-pass filtering if the spectrum of the imaging signals is located near the frequency of the fundamental component or the odd-harmonic components of the HIFU interference. However, this method has a limitation on the spectral bandwidth for an imaging signal. For example, only 2-MHz bandwidth is available for imaging if the center frequency of HIFU is 1 MHz. Additionally, this method requires additional implementation cost, especially for array-based HIFU systems, because electrical pulse generators should be able to generate two electrical signals of 0° and 180° phases with no jitter between the two HIFU signals.

To overcome the limitations, in this paper, we propose another approach to HIFU interference rejection using pulse inversion. Unlike the previous method, the proposed method employs the pulse inversion technique for imaging signals. For one image scanline, an imaging transducer fires ultrasound twice in 0° and 180° phases while HIFUs of the same phase are transmitted in synchronization with the ultrasound transmission for imaging. Because the two sets of the signals received by the imaging transducer contain HIFU interferences in the same phase and imaging signals in 0° and 180° phases, the HIFU interferences can be eliminated after subtracting the two sets of the received signals. In this case, the amplitude of the imaging signal becomes doubled. Additionally, the frequency spectrum of an imaging transducer can be fully used for imaging because no HIFU interference exists in theory. Furthermore, the proposed method is relatively easy to implement because a general ultrasound imaging system has a circuitry for pulse inversion for tissue harmonic imaging. However, the best performance of the proposed method can be achieved when the target is stationary, which is not the case in practice. In the paper, therefore, we demonstrate how to implement the proposed method in a commercial ultrasound scanner and evaluate its imaging performance. In addition, the effect of the target motion on the performance of the proposed HIFU interference rejection is presented.

2. Materials and Methods

2.1. Proposed High-Intensity Focused Ultrasound (HIFU) Interference Elimination and Its Implementation

Figure 1 shows the conceptual diagram of the proposed algorithm for HIFU interference elimination in which two steps of transmission and reception are performed to obtain one HIFU interference-free scanline. In the first step, the HIFU signal and the ultrasound imaging signal with 0° phase are simultaneously transmitted and the imaging transducer with the impulse response of $h_{XDCR}(t)$ receives [17]:

$$\begin{aligned} r_{+}(t) &= \left\{ \left[h_f(t) + h_{odd}(t) + h_{even}(t) \right] + \left[u_f(t) + u_{odd}(t) + u_{even}(t) \right] \right\} * h_{XDCR}(t) \\ &\approx \left[h'_f(t) + h'_{odd}(t) + h'_{even}(t) \right] + u'_f(t) \end{aligned} \tag{1}$$

where $h_f(t)$, $h_{odd}(t)$, and $h_{even}(t)$ are the fundamental, odd, and even harmonic components of the HIFU signal, $u_f(t)$, $u_{odd}(t)$, and $u_{even}(t)$ are those of the ultrasound imaging signal. These signals are the ultrasound waves that are reflected from the tissues and reach the transducer. The asterisk in Equation (1) indicates the convolution operation. Since the full bandwidth of the imaging transducer is used to transmit ultrasound for imaging, only the fundamental component of the imaging signal $u_f{}'(t)$ remains in the received signal. Note that only the fundamental and harmonic components of the HIFU signal of which frequency is in the passband of the imaging transducer remain in the received signal; the components play a role of HIFU interference represented by $h_f{}'(t)$, $h_{odd}{}'(t)$, and $h_{even}{}'(t)$ in Equation (1). The apostrophe in the functions implies the convolutional result between the received ultrasound and the impulse response of the transducer. After T_{PRI} indicating the interval between the ultrasound transmissions with inverted phases, the HIFU signal and the ultrasound imaging signal with 180° phase are simultaneously transmitted and subsequently received. This step can be expressed as:

$$r_-(t - T_{PRI}) \approx \left[h'_f(t - T_{PRI}) + h'_{odd}(t - T_{PRI}) + h'_{even}(t - T_{PRI})\right] + u'_f(t - T_{PRI}). \quad (2)$$

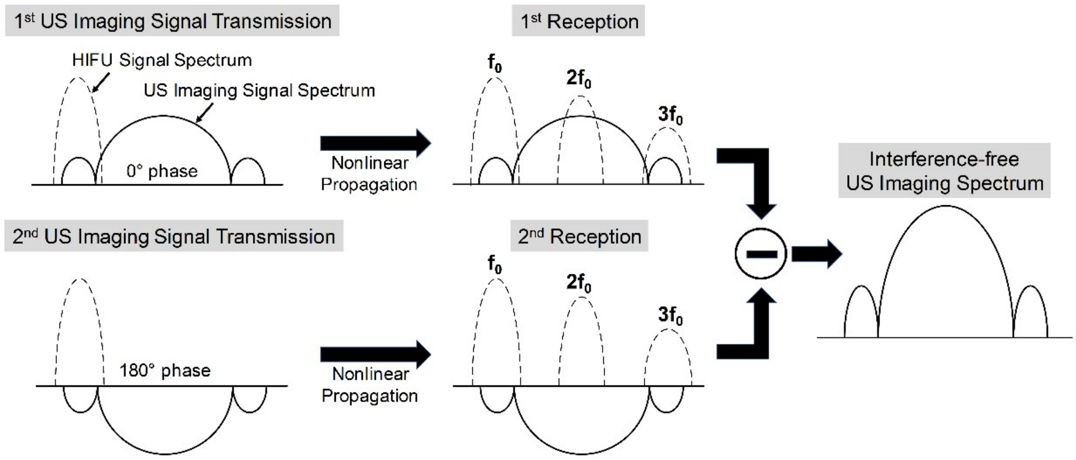

Figure 1. Conceptual diagram of the proposed method for high-intensity focused ultrasound (HIFU) interference elimination.

Since the ultrasound imaging signal has a phase of 180° in the second step of transmission and reception, the fundamental and odd harmonic components of the imaging signal have a negative sign [19]. To obtain one scanline signal, the subtraction of $r_+(t)$ and $r_-(t - T_{PRI})$ is conducted as follows:

$$SL(t) = r_+(t) - r_-(t - T_{PRI}) = \left[h'_f(t) - h'_f(t - T_{PRI})\right] + \left[u'_f(t) - u'_f(t - T_{PRI})\right]. \quad (3)$$

Under the assumption that the target lesion is stationary, i.e.,

$$h'_f(t) = h'_f(t - T_{PRI}) \text{ and } u'_f(t) - u'_f(t - T_{PRI}), \quad (4)$$

Equation (3) becomes:

$$SL(t) = 2u'_f(t), \quad (5)$$

which is a HIFU interference-free scanline signal. In the proposed method, the maximum pulse length of HIFU is less than T_{PRI} because the HIFU and ultrasound imaging signal should be simultaneously transmitted. This means that the pulse repetition of HIFU should be equal to T_{PRI}. Note that the frame rate of monitoring ultrasound imaging decreases at a given number of scanlines as the maximum pulse length of HIFU increases. Equation (5) is an ideal case because in practice the target lesion moves between the successive transmission and reception events, i.e., T_{PRI} due to patient motion and breathing during HIFU surgery. This hampers the complete elimination of the HIFU interference signal. The amount of residual HIFU interference after the subtraction of $r_+(t)$ and $r_-(t - T_{PRI})$ depends on how fast the target lesion is moving; their relationship will be demonstrated below.

The proposed method for HIFU interference elimination was implemented in a commercial ultrasound research imaging scanner (Vantage 128, Verasonics Inc., Redmond, WA, USA) that has an option to change the polarity of transmit pulse. This option facilitated the transmission of ultrasound imaging signals with 0° and 180° phases. Note that this scheme allows the full bandwidth of an imaging transducer to be used for ultrasound transmission unlike the conventional pule inversion for tissue harmonic imaging because the harmonics generated by the ultrasound imaging signals do not have to be received. Additionally, this imaging scanner has the ability to write radio-frequency (RF) data to local buffer memory and add new RF data to the RF data previously stored in the local buffer memory, which is called the write/accumulation mode. The subtraction of two sets of received RF data in Equation (3) was implemented using the receive apodization function provided by the scanner and the write/accumulation mode as shown in Figure 2; the negative apodization means multiplying RF data by -1, thus reversing the phase of the RF data. For one scanline, the RF signal received after the first transmission and reception step, i.e., $r_+(t)$ is stored in the local buffer memory. In this step, the ultrasound transmission is conducted using the positive polarity of transmit pulse and the phase of the received RF data does not change because of the positive apodization (i.e., multiplying the RF data by +1). In the second transmission and reception step, the negative polarity of transmit pulse is used for ultrasound transmission and the phase of the received RF data is reversed using the negative apodization before adding the new RF data to the RF data previously stored in the local buffer memory. This procedure is repeated until all local buffer memories corresponding to a predetermined number of scanlines are filled with RF data. After this step, beam formation is performed to obtain the scanlines expressed as Equation (3). These scanline data are used to construct an ultrasound monitoring image by means of the echo-processing functions provided by the ultrasound research imaging scanner; a 41-tap band-pass filter with cutoff frequencies of 2.2 and 5 MHz is used to remove out-of-band noise of the scanline signals.

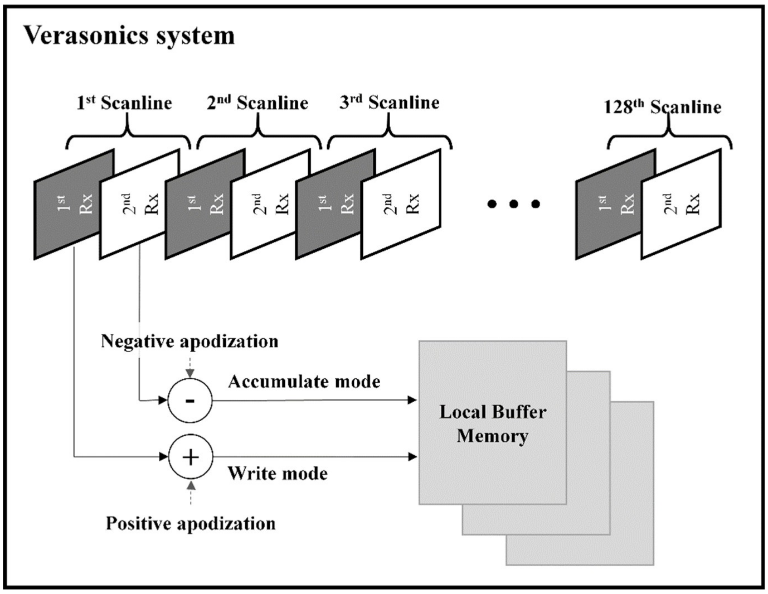

Figure 2. Functional block diagram for the real-time HIFU interference elimination method implemented in a commercial ultrasound scanner. Rx stands for ultrasound reception.

2.2. Experimental Arrangement

An experimental arrangement was set to verify and evaluate the proposed method as shown in Figure 3. For the simultaneous delivery of HIFU and ultrasound for imaging, the ultrasound imaging system in which the proposed method had been implemented was modified to generate a trigger signal whenever ultrasound was transmitted for imaging. This trigger signal was sent to a function generator (AFG3252, Tektronix Inc., Beaverton, OR, USA) that was responsible for generating a 1.1 MHz sinusoid wave with a pulse length of 136 µs. T_{PRI} was set to be 500 µs, which means that the pulse repetition time of HIFU was also 500 µs and the duty cycle was 27.2%. Since the monitoring ultrasound images consisted of 128 scanlines, the frame rate was 7.8 Hz. The 1.1 MHz sinusoid signal was amplified by 49 dB with a RF power amplifier (75A250A, Amplifier Research Corp., Souderton, PA, USA) and passed to a ring-shaped HIFU transducer (H102, Sonic Concepts, Bothell, WA, USA) through an impedance matching network; the electrical signal with a voltage of 70 $V_{\text{peak-peak}}$ was used to generate HIFU. A convex array (C5-2, Verasonics Inc., Redmond, WA, USA) used for ultrasound imaging was placed in the central opening of the HIFU transducer. As a target, an excised bovine liver was placed on a 55 mm high BSA (bovine serum albumin) phantom immersed in a deionized-water-filled container. The distance between the convex array and the bottom of the phantom was 130 mm. Note that the fabrication process of the BSA phantom can be found in [20]. The HIFU and imaging transducers were also immersed in the deionized-water-filled container to induce coagulation in the bovine liver while acquiring ultrasound monitoring images. Note that the synchronized transmission of HIFU and imaging ultrasound was controlled by the imaging system as described above. Since the imaging system has a pulse inversion function with a minimal jitter between two imaging ultrasounds with a 180° phase difference, it is possible to avoid the problem of image quality deterioration due to asynchronous transmission. If two HIFU pulses with phase 0° and 180° are transmitted as in the previously proposed method, a HIFU system should have a jitter removal circuit. Otherwise, white straight lines may appear in ultrasound images [16].

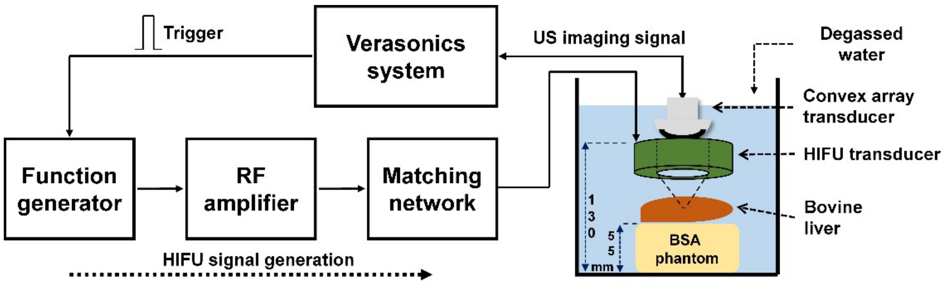

Figure 3. Experimental arrangement for performance evaluation of the implemented HIFU interference elimination method.

Another experimental setup was constructed to ascertain the effect of target motion on the performance of the proposed method for HIFU interference elimination as shown in Figure 4. When the ultrasound image of a moving target is acquired, the target position changes every pulse repetition interval, i.e., T_{PRI} for imaging. Therefore, residual HIFU interference signal increases when a target moves quickly at a given T_{PRI}. This is also true when T_{PRI} is increased at a given target motion speed. To mimic this situation, a 0.9 mm diameter graphite rod serving as a target was inserted in the BSA phantom. The graphite-contained phantom was placed in the deionized-water-filled container on a motorized stage (SGSP160-YAW, SIGMAKOKI Co. Ltd., Tokyo, Japan). In the beginning, the graphite rod was located at the focal length of the HIFU transducer, i.e., 62.6 mm. A pulse-echo signal $r_+(t)$ (i.e., ultrasound A-mode signal) was acquired after transmitting ultrasound with a phase of 0° while delivering HIFU, which is called a reference in this paper. In the next step, both HIFU and ultrasound with a phase of 180° were simultaneously delivered to the target located at the same position to obtain $r_-(t - T_{PRI})$. Since the target position did not change, the assumption for Equation (5) is valid: $h'(t) = h'(t - T_{PRI})$ and $u_f{}'(t) = u_f{}'(t - T_{PRI})$. Another A-mode signal was acquired after moving the target up by 5 µm and subsequently transmitting both HIFU and ultrasound with a phase of 180° at the same time; 20 A-mode signals were acquired while moving the target in 5 µm increments. When the reference and these A-mode signals were used to obtain each scanline, the assumption was not valid and residual HIFU interference existed in the scanline signal. For quantitative analysis of residual HIFU interference as a function of target motion distance, correlation coefficients between the reference scanline and other scanline signals were calculated. Note that the reference scanline signal is defined as a signal obtained using the reference and the A-mode signal acquired in the case of no target motion. Additionally, the energy of each scanline was calculated by squaring and summing the scanline signals that were acquired using the oscilloscope. It was expected that the energy would increase as residual HIFU interference increases. The experiment was repeated 5 times to calculate the mean and standard deviation of both correlation coefficient and scanline energy.

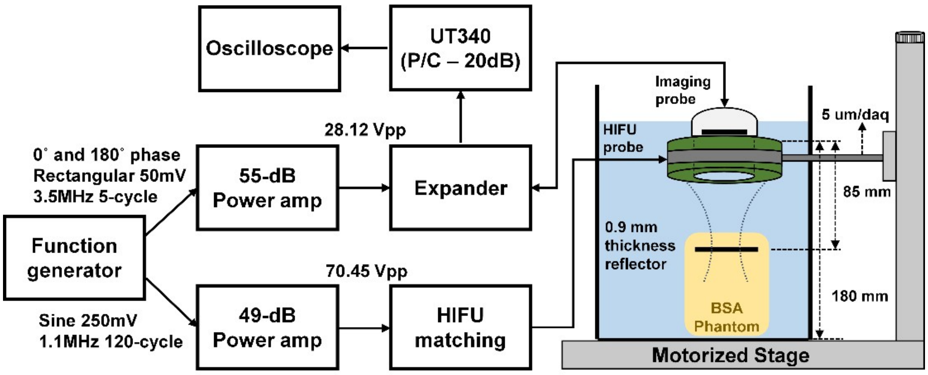

Figure 4. Experimental arrangement to ascertain the effect of target motion on the performance of the proposed method.

For this experiment of investigating the target motion effect, a single-element ultrasound transducer (NDT, Olympus Corp., Waltham, MA, USA) with a center frequency of 3.5 MHz and a −6 dB bandwidth of 2.5 MHz was used instead of the convex array. This transducer was completely inserted in the central opening of the HIFU transducer to acquire ultrasound A-mode signals. By doing so, the strong echoes from the rear surface of the HIFU transducer and the side of its hole, that occurred when the convex array was used, could be avoided. In addition, the single-element transducer facilitated placing the graphite rod in the on-axis beam profile regardless of moving the target, as compared to the convex array. A two-channel function generator (AFG3252, Tektronix Inc., Beaverton, OR, USA) was used to generate a 3.5-MHz, 5-cycle rectangular-shaped electrical pulse for the monitoring signal (i.e., a pulse length of about 1.42 µs) and a 1.1-MHz, 120-cycle sinusoid signal for HIFU (i.e., a pulse length of about 109 µs). These signals were amplified to 28.12 $V_{peak\text{-}peak}$ for the monitoring signal and 70.45 $V_{peak\text{-}peak}$ for HIFU by using two RF power amplifiers (75A250A, Amplifier Research Corp., Souderton, PA, USA; A150, ENI Corp., Rochester, NY, USA). The monitoring signal reflected from the graphite rod was received by a pulse-receive system (UT340, UTEX Scientific Instruments Inc., Mississauga, ON, Canada) in the pitch-catch mode with an amplified gain of 20 dB. An oscilloscope (DPO7054, Tektronix Inc., Beaverton, OR, USA) was used to record the received monitoring signal. A customized expander was used to protect the pulse-receive system from the high voltage output of the 55-dB power amplifier. The DC cancellation was conducted using a 257-tap band-pass filter to remove out-of-band noise of the scanline signals [21]; its cutoff frequencies were 2.5 and 4 MHz. All signal processing was conducted using MATLAB (Math-Works Inc., Natick, MA, USA).

3. Results

3.1. Real-Time HIFU Treatment Monitoring

Ultrasound monitoring images of the induction of thermal coagulation in the excised bovine liver were obtained before and after the application of the proposed method (see video clips in the Supplementary Materials). As shown in Figure 5a, strong HIFU interference appeared in the ultrasound monitoring image when the proposed method was not used. In this case, it was difficult to observe echogenicity change in the bovine liver. In contrast, the HIFU interference disappeared when the proposed method was applied. This made it possible to monitor the treatment area during the treatment period. In Figure 5b obtained before HIFU insonation, the solid white arrow indicates the boundary of the water and bovine liver. Note that the bright spots of which intensity was not changed with time appeared in the video clips and Figure 5 (see the dashed arrows in Figure 5b). These are the reverberation artifacts generated at the rear surface of the HIFU transducer and the side of its hole, which occurred because the central opening of the HIFU transducer was too small to allow the convex imaging probe to be inserted completely into the opening (see Figure 3). At 5 s after the HIFU insonation, the echogenicity change indicated by the dashed white arrows and the tissue boundary were clearly observed (see Figure 5c). The hyperechoic spot appearing during the HIFU exposure (indicated by the dashed circle in Figure 5d) is mainly due to microbubbles induced by the HIFU [7,22] and partially acoustic impedance change of the region due to coagulation [23,24]. Since some microbubbles disappear without tissue damage after cessation of the HIFU exposure [22], the size of the hyperechoic spot may not match the actual size of the coagulation lesion measured in the tissue (see Figure 6). However, the ultrasound monitoring image provided the information about the location and echogenicity change of the treatment area. As a result, the experimental results imply that the proposed method enables us to confirm the focal area of HIFU and to monitor the echogenicity changes of the area due to its capability of real-time HIFU interference elimination. Additionally, this result implies that the proposed method can help the thermometry [6] and echo decorrelation [25,26] methods accurately visualize and measure the treatment area in real time because these methods require a high signal-to-noise ratio to achieve high accuracy. For this reason, the cessation of HIFU exposure is currently necessary at the time of measurement.

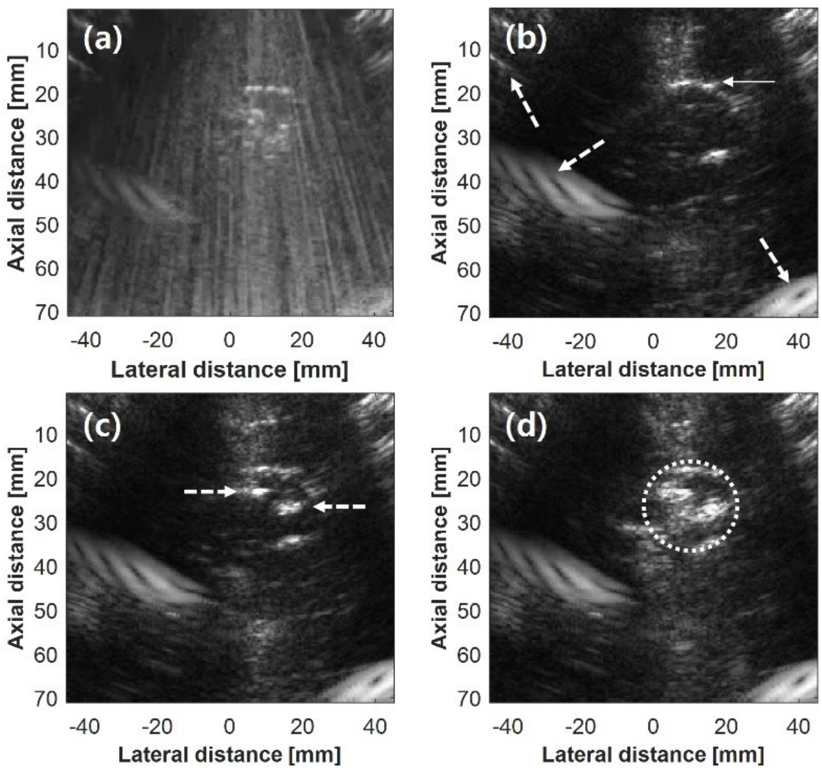

Figure 5. (**a**) Ultrasound monitoring images of the excised bovine liver obtained before the application of the proposed method. The HIFU interference disappeared when the proposed method was applied: (**b**) 0 s, (**c**) 5 s, and (**d**) 15 s after HIFU insonation. In (**b**), the solid white arrow indicates the boundary of the water and bovine liver and the dashed white arrows indicate reverberation images at the rear surface of the HIFU transducer and the side of its hole. In (**c**), the echogenicity change is indicated by the dashed white arrows. The dotted white circle indicates the predicted treatment area in (**d**).

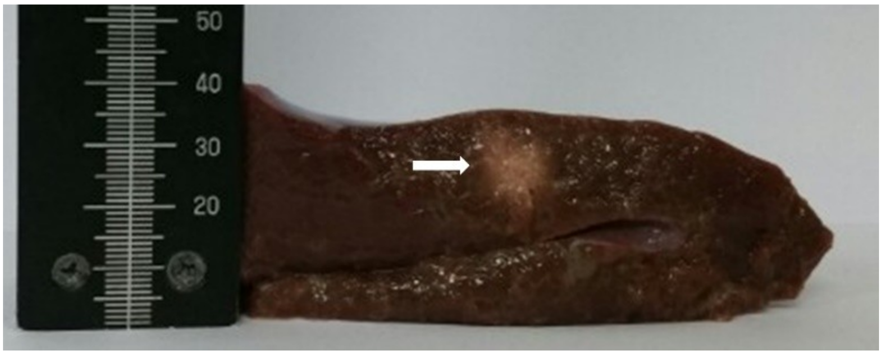

Figure 6. Photograph of the lesion formation induced in the excised bovine liver, which corresponds to the dotted white circle shown in Figure 5d.

3.2. Effect of Target Motion on the Performance of the Proposed Method

The A-mode signals were obtained by the proposed pulse-inversion method while moving the target in 5 μm increments to ascertain the effect of target motion on the performance of the proposed HIFU interference elimination method. For the purpose of comparison, the A-mode signal and its frequency spectrum were also acquired without HIFU delivery as shown in Figure 7a,b. The three signal peaks appeared in the A-mode signal: the first peak signal generated at the interface between the water and phantom surface, the second at the graphite rod, and the third at the bottom of the phantom. When HIFU and ultrasound were simultaneously transmitted under the condition where the target was not moved, only a very small amount of the HIFU interference was observed in the A-mode signal (see Figure 7c) because the proposed method effectively eliminated the HIFU interference. From Figure 7d and Table 1, it was learned that the HIFU interference signal appeared mainly in the out-of-band of the spectrum of the monitoring ultrasound signal in this case; the fundamental, second harmonic, and fourth harmonic components of the HIFU interference signal located at 1.1, 2.2, and 4.4 MHz primarily affected the increase in the spectral magnitude. The magnitude at its third harmonic frequency (i.e., 3.3 MHz) similar to the center frequency of the monitoring ultrasound transducer increased by only 1.12 dB. However, the HIFU interference signal increased as the distance of the target motion increased. When the target was moved by 10, 30, 50 μm after transmitting and receiving ultrasound with a phase of 0°, the considerable amount of the HIFU interference remained in the A-mode signals as shown in Figure 8; the fundamental, second harmonic, third harmonic, and fourth harmonic signals of the HIFU interference predominantly appeared in the frequency spectra. From Figures 7 and 8, it was seen that the HIFU echoes received by the transducer were generated from the scatterers in the phantom as well as the graphite rod. The HIFU interference signals appeared after the first peak signal corresponding to the interface between the water and phantom when the interference signals were not effectively removed. However, the amplitude of the HIFU interferences from the region between the phantom surface and the graphite rod was relatively low because the density of the scatterers was possibly low in this region, which frequently occurs in custom-made phantoms.

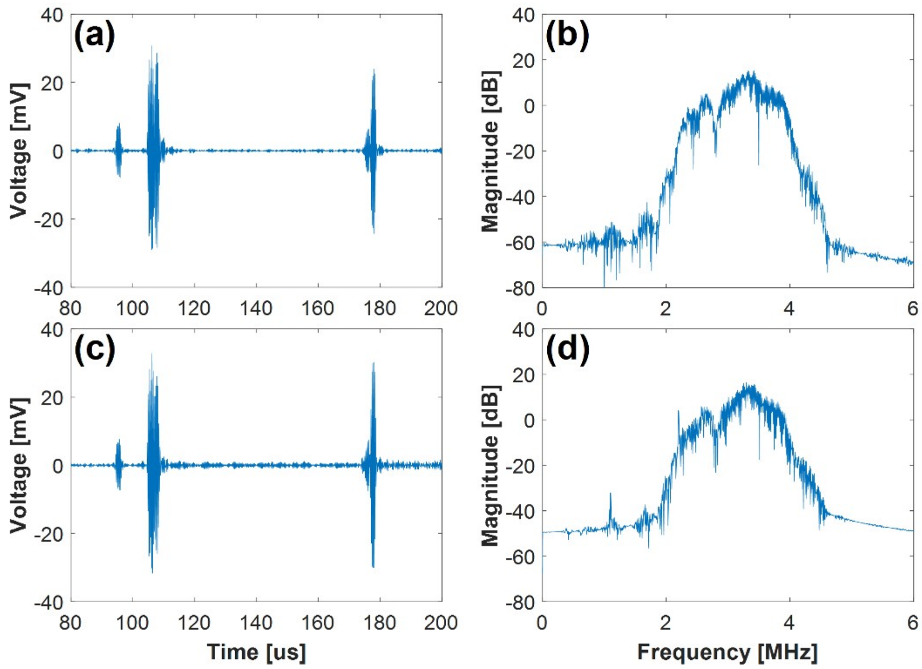

Figure 7. A-mode signal and its frequency spectrum obtained after transmitting the ultrasound imaging signal only (**a**,**b**) and those obtained after transmitting both HIFU and the ultrasound imaging signal without the target motion (**c**,**d**).

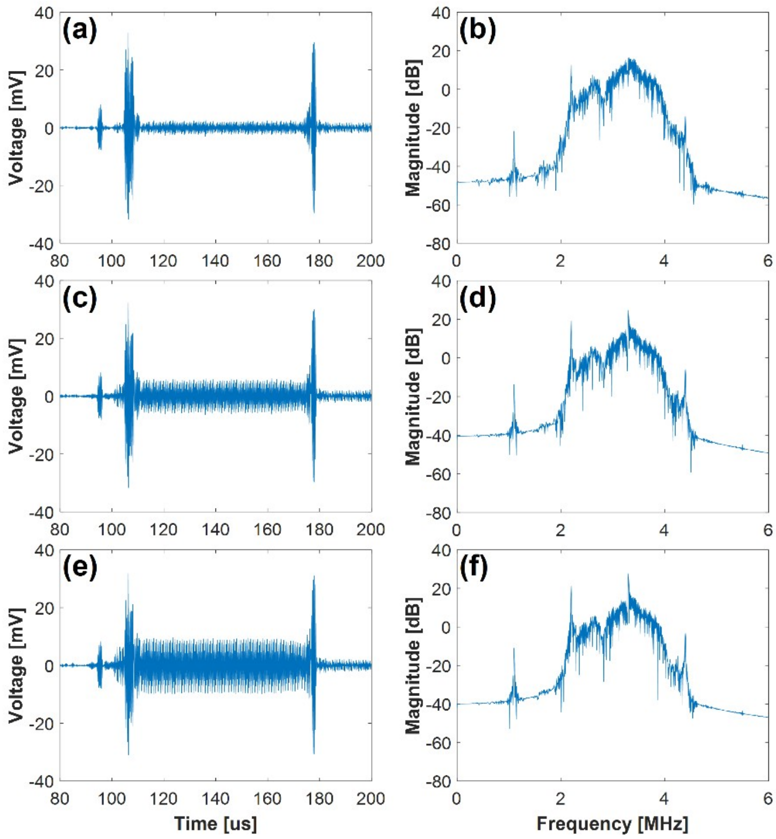

Figure 8. A-mode signal and its frequency spectrum obtained after transmitting both HIFU and the ultrasound imaging signal in the case of a moving distance of 10 μm (**a**,**b**), 30 μm (**c**,**d**), and 50 μm (**e**,**f**).

Table 1. Spectral magnitude at the fundamental and harmonic frequencies of the transmitted HIFU, which was measured from the frequency spectra of the A-mode signals in Figures 6 and 7. λ is the wavelength of the 1.1 MHz HIFU transducer, which was calculated at a sound speed of 1540 m/s.

Condition	Moving Distance (µm)	Magnitude (dB)			
		1.1 MHz	**2.2 MHz**	**3.3 MHz**	**4.4 MHz**
Ultrasound Only	-	−54.32	−13.92	15.25	−40.84
Ultrasound + HIFU	0	−32.10	4.06	16.37	−26.78
	10 (0.071λ)	−21.80	12.64	16.29	−14.23
	30 (0.214λ)	−13.79	19.24	24.72	−5.93
	50 (0.357λ)	−11.08	21.34	27.73	−3.26
	100 (0.714λ)	−4.84	26.12	34.17	2.86

For quantitative analysis, correlation coefficients between the reference scanline and other scanline signals were calculated as a function of the target moving distance. As shown in Figure 9a, the correlation coefficient was gradually decreased as the target moving distance increased; the decrease rate was 1.9%, 4.8%, and 7.1% in the cases of a moving distance of 5, 10, and 15 µm. This value was 19.8%, 39%, and 66.9% at a moving distance of 30, 50, and 100 µm (see Table 2). This result indicates that an increase in target motion leads to reducing the efficiency of the proposed method in HIFU interference elimination and this adverse effect becomes more dominant after a moving distance of 30 µm. The remaining HIFU interference acts as a noise, thus decreasing a signal-to-noise ratio of monitoring ultrasound signal. As shown in Figure 9b and Table 2, the energy of the remaining HIFU interference was exponentially increased as the target moving distance increased. Note that the energy was increased by only 4% when the moving distance was changed to 10 µm (i.e., from 0.173 ± 0.003 to 0.180 ± 0.003). The results in Figure 9 were obtained under the condition of 1.1 MHz HIFU (i.e., a wavelength of 140 µm) and can be generalized by normalizing the moving distance to the wavelength as shown in Table 2. Note that the change in the center frequency of an imaging transducer has nothing to do with the efficiency of HIFU interference elimination although the axial resolution of monitoring images may be degraded at a given moving distance of the target.

Table 2. Correlation coefficient between the reference scanline and other scanline signals and energy of each scanline. The measured values are expressed as mean ± standard deviation. λ is the wavelength of the 1.1 MHz HIFU transducer, which was calculated at a sound speed of 1540 m/s.

	Moving Distance (µm)				
	0	**10 (0.071λ)**	**30 (0.214λ)**	**50 (0.357λ)**	**100 (0.714λ)**
Correlation	1.000 ± 0.005	0.952 ± 0.014	0.802 ± 0.046	0.643 ± 0.035	0.331 ± 0.034
Energy	0.173 ± 0.003	0.180 ± 0.003	0.234 ± 0.015	0.366 ± 0.023	1.029 ± 0.091

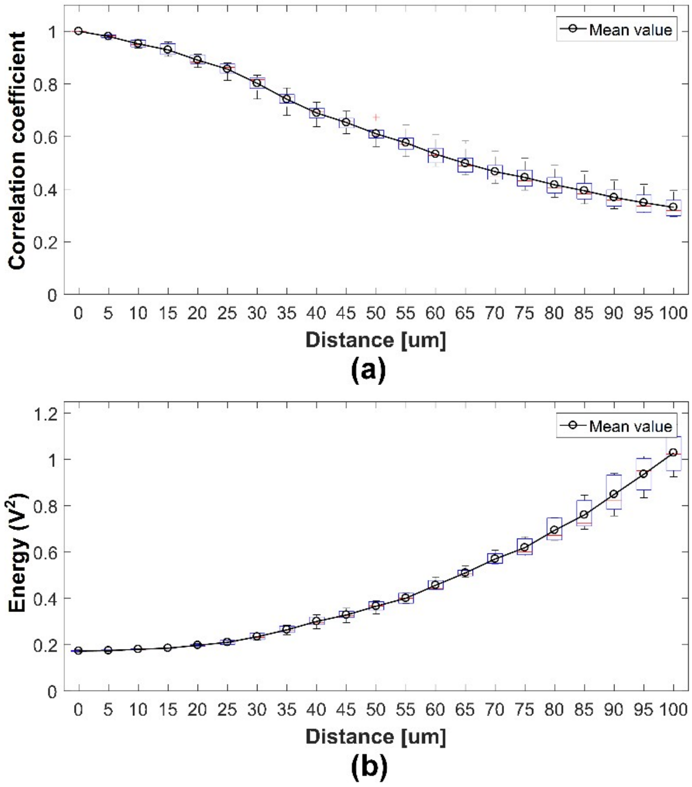

Figure 9. Boxplots of (**a**) correlation coefficients between the reference scanline and other scanline signals and (**b**) energy of each scanline calculated by squaring and summing the scanline signals as a function of the target moving distance. Note that the scanline signals were acquired using the oscilloscope.

4. Discussion

The basic assumption for the proposed method is that the target lesion is stationary. In practice, however, tissue motion in response to heart beat, respiration, and patient motion happens. This causes an increase in residual HIFU interference because two HIFU interference signals acquired in between the time interval of T_{RPI} are not equal to each other and the HIFU inference is not completely removed. From the experimental results, it can be concluded that the discrepancy between the two HIFU interference signals depends on a target moving a distance in the axial direction, thus increasing the amount of remaining HIFU interference. Note that in this study only the axial motion of the target was considered because the fundamental and odd harmonic elimination efficiency of the pulse inversion method is more influenced by the axial motion of the target than the lateral motion [27]. The efficiency of the HIFU interference signals and the harmonic elimination is closely related to the phase aberration between the two sets of echoes obtained between the time intervals of T_{PRI}. The phase aberration occurs much less when a target moves in the lateral direction than the axial direction [28]. Although target motion causes HIFU interference to remain in ultrasound monitoring signals, the moving distance up to 10 μm is not expected to have a significant effect on the quality of ultrasound monitoring images based on the experimental results; this can also be seen in the ultrasound monitoring images of the tissue mimicking phantom (see Figure 10). Note that this phantom did not contain the graphite rod because the remaining HIFU interferences occur in the scattering region as shown in Figure 8. When the phantom was not moved, the ultrasound image obtained after simultaneous delivery of ultrasound and HIFU (Figure 10b) was similar to the image obtained under the condition of no HIFU (Figure 10a). Additionally, we could observe the speckle pattern in the phantom in the ultrasound image related to a target moving distance of 10 μm (Figure 10c) although a small amount of the remaining HIFU interference appeared in the image. This indicates that the residual HIFU interference had a magnitude smaller than the speckles. In contrast, it was difficult to recognize the speckle pattern in the ultrasound image when the target was moved by 50 μm (Figure 10d).

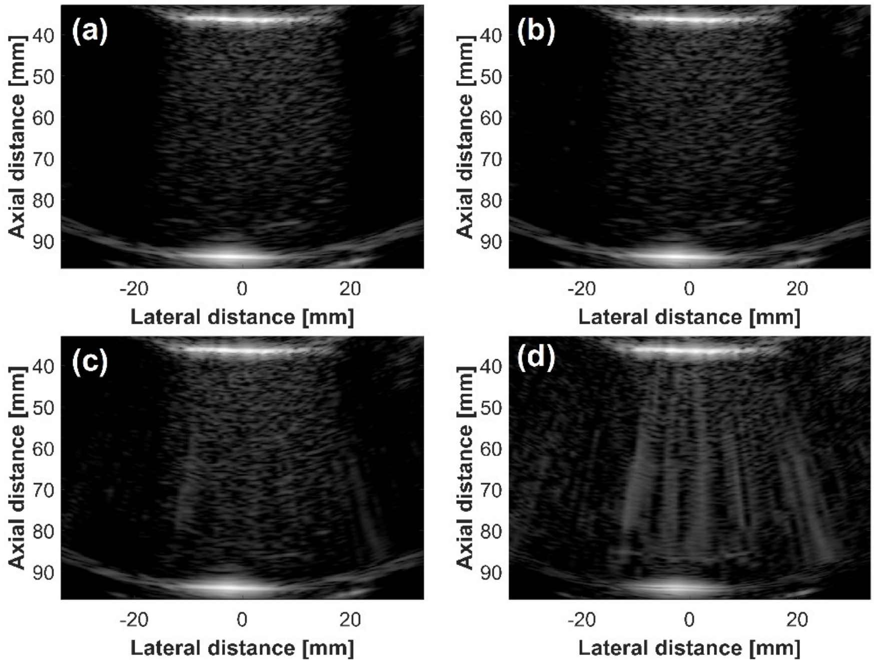

Figure 10. Ultrasound B-mode images of the tissue-mimicking phantom in the cases of (**a**) no HIFU exposure, (**b**) HIFU exposure but no target motion, (**c**,**d**) HIFU exposure after moving the target by (**c**) 10 μm and (**d**) 50 μm.

The fastest moving organ in the body is the heart and the maximum moving velocity is reported as 25 cm/s [29]. This velocity corresponds to a target moving distance of 32.5 μm under the condition where the frame rate of ultrasound imaging is 30 frames/s in the case of pulse inversion and the number of scanlines for an image is 128 (i.e., 0.25 × T_{PRI}). Note that two transmissions of a scanline should be conducted for the proposed method and thus T_{PRI} is calculated as 130 μs (i.e., 1/(2 × 30 × 128)). In this case, unremoved HIFU interference may lead to degradation of ultrasound image quality. However, the heart is not the target organ for current HIFU surgery. On the other hand, the maximum moving velocity of the liver due to respiratory organ motion is 10 mm/s [27] that corresponds to a target moving distance of 1.3 μm (i.e., 0.01 × T_{PRI}). If the frame rate is reduced to 15 frames/s for pulse inversion imaging of a deep-lying target, this target moving distance is changed to only 2.6 μm because T_{PRI} is doubled. Therefore, it can be concluded that the organs in the abdomen such as the liver are considered to be stationary and the basic assumption for the proposed method is valid. If a target moving distance of 10 μm is acceptable for construction of ultrasound monitoring images, the proposed method can be used to monitor HIFU surgery for the organs of which maximum moving velocity is up to 7.7 cm/s (i.e., 10/T_{PRI}) when HIFU has a center frequency of 1.1 MHz and T_{PRI} is 130 μs.

In addition to the target motion, the cavitation induced by HIFU may make it possible that the difference between the HIFU interference signals obtained in the successive transmission and reception events becomes large and thus the elimination efficiency may be considerably degraded, although this was not observed in this study (see Figure 5 and video clips in the Supplementary Materials). The cavitation may lead to an increase in magnitude of the fundamental and harmonic frequencies of the HIFU interference remaining after the inference elimination by the proposed method. In this case, a few notch filters can be used to further remove the remaining HIFU interference [14] because its fundamental and harmonic frequencies are known and their spectral bandwidths are typically narrow.

One requirement for the proposed method is simultaneous transmission of HIFU for therapy and ultrasound for monitoring. For this reason, T_{PRI} determines the maximum pulse length of HIFU as well as the frame rate of monitoring imaging; the duty cycle defined as the ratio of the HIFU pulse length over T_{RPI} serves as one of the HIFU operation parameters. Therefore, the frame rate inevitably decreases if HIFU pulse is elongated to increase acoustic energy. Furthermore, the proposed method cannot be directly used for continuous-wave HIFU treatment because the essential requirement cannot be met. As a remedy, HIFU with a high duty cycle such as 99% can be used instead of continuous-wave HIFU without reducing the frame rate [17]. This long HIFU wave causes a portion of the HIFU interference generated by the current HIFU transmission to be received at the next transmission and reception event. This phenomenon can also occur due to the reverberation of HIFU. The previously proposed method [16] in which two HIFU pulses with phases 0° and 180° are transmitted had the same problem. To overcome this problem, a new pulse sequence in which three HIFU pulses with phases of 0°, 180°, and 0° were subsequently transmitted and received for one scanline has been proposed, and we have shown that the pulse sequence can efficiently remove HIFU interference even at a high duty cycle such as 90% [17]. This pulse sequence can be also employed for the method proposed here to solve the same problem.

5. Conclusions

In this paper, we have proposed a real-time HIFU treatment monitoring method based on pulse inversion of ultrasound for imaging. The advantage of the proposed method over the previously reported pulse inversion-based HIFU treatment monitoring method is to use the full frequency spectrum of an imaging transducer because there is no HIFU interference in theory. This means that the axial resolution of ultrasound images is not lowered. Another benefit is that the proposed method can be easily implemented in a commercial ultrasound scanner with minimal modification, which was demonstrated using the ultrasound research scanner in this study. Additionally, it was demonstrated that the proposed method works well even when maximum target moving velocity is up to 7.7 cm/s (or 0.071λ) in the case where HIFU has a center frequency of 1.1 MHz and T_{PRI} is 130 µs, although the target organs of HIFU surgery can be considered to be stationary. Based on the experimental results, we believe that the proposed method can be used for real-time HIFU surgery monitoring that is a pivotal function for maximized treatment efficacy.

Supplementary Materials: The following are available online at http://www.mdpi.com/2076-3417/8/11/2219/s1, Video S1: Ultrasound treatment monitoring images without the proposed method, Video S2: Ultrasound treatment monitoring images with the proposed method.

Author Contributions: conceptualization, supervision, and funding acquisition, J.H.C.; methodology, E.-J.S., B.K. and J.H.C.; software, E.-J.S. and B.K.; validation, E.-J.S., B.K. and J.H.C.; investigation, E.-J.S. and B.K.; writing—original draft preparation, E.-J.S.; writing—review and editing, J.H.C., E.-J.S. and B.K.

Funding: This research was supported by the National Research Foundation of Korea (NRF) funded by the Ministry of Science and ICT (NRF-2017R1A2B2002838).

Conflicts of Interest: The authors declare no conflict of interest.

References

1. Leinenga, G.; Götz, J. Scanning ultrasound removes amyloid-β and restores memory in an Alzheimer's disease mouse model. *Sci. Transl. Med.* **2015**, *7*, 278ra33. [CrossRef] [PubMed]
2. Meng, Y.; Volpini, M.; Black, S.; Lozano, A.M.; Hynynen, K.; Lipsman, N. Focused ultrasound as a novel strategy for Alzheimer's disease therapeutics. *Ann. Neurol.* **2017**, *81*, 611–617. [CrossRef] [PubMed]
3. MacGregor, J.L.; Tanzi, E.L. Microfocused ultrasound for skin tightening. *Semin. Cutan. Med. Surg.* **2013**, *32*, 18–25. [PubMed]
4. Jang, J.; Chang, J.H. Design and fabrication of double-focused ultrasound transducers to achieve tight focusing. *Sensors* **2016**, *16*, 1248. [CrossRef] [PubMed]

5. Solovchuk, M.A.; Hwang, S.C.; Chang, H.; Thiriet, M.; Sheu, T.W.H. Temperature elevation by HIFU in ex vivo porcine muscle: MRI measurement and simulation study. *Med. Phys.* **2014**, *41*, 052903. [CrossRef] [PubMed]
6. Liu, D.; Ebbini, E.S. Real-time 2-D temperature imaging using ultrasound. *IEEE Trans. Biomed. Eng.* **2010**, *57*, 12–16. [PubMed]
7. Vaezy, S.; Shi, X.; Martin, R.W.; Chi, E.; Nelson, P.I.; Bailey, M.R.; Crum, L.A. Real-time visualization of high-intensity focused ultrasound treatment using ultrasound imaging. *Ultrasound Med. Biol.* **2001**, *27*, 33–42. [CrossRef]
8. Wu, C.C.; Chen, C.N.; Ho, M.C.; Chen, W.S.; Lee, P.H. Using the acoustic interference pattern to locate the focus of a high-intensity focused ultrasound (HIFU) transducer. *Ultrasound Med. Biol.* **2008**, *34*, 137–146. [CrossRef] [PubMed]
9. Kuroda, K. MR techniques for guiding high-intensity focused ultrasound (HIFU) treatments. *J. Magn. Reson. Imaging* **2018**, *47*, 316–331. [CrossRef] [PubMed]
10. Tanter, M.; Pernot, M.; Aubry, J.F.; Montaldo, G.; Marquet, F.; Fink, M. Compensating for bone interfaces and respiratory motion in high-intensity focused ultrasound. *Int. J. Hyperther.* **2007**, *23*, 141–151. [CrossRef]
11. Nandlall, S.D.; Jackson, E.; Coussios, C.C. Real-time passive acoustic monitoring of HIFU-induced tissue damage. *Ultrasound Med. Biol.* **2011**, *37*, 922–934. [CrossRef] [PubMed]
12. Owen, N.R.; Bailey, M.R.; Hossack, J.; Crum, L.A. A method to synchronize high-intensity, focused ultrasound with an arbitrary ultrasound imager. *IEEE Trans. Ultrason. Ferroelectr. Freq. Control* **2006**, *53*, 645–650. [CrossRef] [PubMed]
13. Pichardo, S.; Gelet, A.; Curiel, L.; Chesnais, S.; Chapelon, J.Y. New integrated imaging high intensity focused ultrasound probe for transrectal prostate cancer treatment. *Ultrasound Med. Biol.* **2008**, *34*, 1105–1116. [CrossRef] [PubMed]
14. Jeong, J.S.; Chang, J.H.; Shung, K.K. Ultrasound transducer and system for real-time simultaneous therapy and diagnosis for noninvasive surgery of prostate tissue. *IEEE Trans. Ultrason. Ferroelectr. Freq. Control* **2009**, *56*, 1913–1922. [CrossRef] [PubMed]
15. Jeong, J.S.; Chang, J.H.; Shung, K.K. Pulse compression technique for simultaneous HIFU surgery and ultrasonic imaging: A preliminary study. *Ultrasonics* **2012**, *52*, 730–739. [CrossRef] [PubMed]
16. Song, J.H.; Yoo, Y.; Song, T.K.; Chang, J.H. Real-time monitoring of HIFU treatment using pulse inversion. *Phys. Med. Biol.* **2013**, *58*, 5333–5350. [CrossRef] [PubMed]
17. Song, J.H.; Chang, J.H. An effective pulse sequence for simultaneous HIFU insonation and monitoring. *IEEE Trans. Ultrason. Ferroelectr. Freq. Control* **2014**, *61*, 1580–1587. [CrossRef] [PubMed]
18. Ma, Q.; Ma, Y.; Gong, X.; Zhang, D. Improvement of tissue harmonic imaging using the pulse-inversion technique. *Ultrasound Med. Biol.* **2005**, *31*, 889–894. [CrossRef] [PubMed]
19. Shen, C.C.; Chou, Y.H.; Li, P.C. Pulse inversion techniques in ultrasonic nonlinear imaging. *J. Med. Ultrasound* **2005**, *13*, 3–17. [CrossRef]
20. Kim, H.; Kang, J.; Chang, J.H. Thermal therapeutic method for selective treatment of deep-lying tissue by combining laser and high-intensity focused ultrasound energy. *Opt. Lett.* **2014**, *39*, 2806–2809. [CrossRef] [PubMed]
21. Chang, J.H.; Sun, L.; Yen, J.T.; Shung, K.K. Low-cost, high-speed back-end processing system for high-frequency ultrasound B-mode imaging. *IEEE Trans. Ultrason. Ferroelectr. Freq. Control* **2009**, *56*, 1490–1497. [CrossRef] [PubMed]
22. Kim, H.; Chang, J.H. Increased light penetration due to ultrasound-induced air bubbles in optical scattering media. *Sci. Rep.* **2017**, *7*, 16105. [CrossRef] [PubMed]
23. Shishitani, T.; Yoshizawa, S.; Umemura, S.I. Acoustic impedance evaluation of high-intensity-focused-ultrasound exposed chicken breast muscle using ultrasonic microscopy. *Jpn. J. Appl. Phys.* **2010**, *49*, 07HF04. [CrossRef]
24. Kim, H.; Jo, G.; Chang, J.H. Ultrasound-assisted photothermal therapy and real-time treatment monitoring. *Biomed. Opt. Express* **2018**, *9*, 4472–4480. [CrossRef]
25. Abbass, M.A.; Killin, J.K.; Mahalingam, N.; Hooi, F.M.; Barthe, P.G.; Mast, T.D. Real-time spatiotemporal control of high-intensity focused ultrasound thermal ablation using echo decorrelation imaging in ex vivo bovine liver. *Ultrasound Med. Biol.* **2018**, *44*, 199–213. [CrossRef] [PubMed]

26. Abbass, M.A.; Garbo, A.J.; Mahalingam, N.; Killin, J.K.; Mast, T.D. Optimized echo decorrelation imaging feedback for bulk ultrasound ablation control. *IEEE Trans. Ultrason. Ferroelectr. Freq. Control* **2018**, *65*, 1743–1755. [CrossRef] [PubMed]
27. Shen, C.C.; Li, P.C. Motion artifacts of pulse inversion-based tissue harmonic imaging. *IEEE Trans. Ultrason. Ferroelectr. Freq. Control* **2002**, *49*, 1203–1211. [CrossRef] [PubMed]
28. Kim, K.S.; Hwang, J.S.; Jeong, J.S.; Song, T.K. An efficient motion estimation and compensation method for ultrasound synthetic aperture imaging. *Ultrason. Imaging* **2002**, *24*, 81–99. [CrossRef] [PubMed]
29. Davies, S.C.; Hill, A.L.; Holmes, R.B.; Halliwell, M.; Jackson, P.C. Ultrasound quantitation of respiratory organ motion in the upper abdomen. *Br. J. Radiol.* **1994**, *67*, 1096–1102. [CrossRef] [PubMed]